Using Real Time Phase contrast MRI to investigate CSF oscillations and aqueductal pressure gradients during free breathing

Pan LIU, Kimi Owashi, Cyrille Capel, Serge Metanbou, Olivier Balédent

Using Real Time Phase contrast MRI to investigate CSF oscillations and aqueductal pressure gradients during free breathing

Pan Liu[1,2], Kimi Owashi[1], Serge Metanbou[3], Cyrille Capel[1,4], Olivier Balédent[1,2]

[1] CHIMERE UR 7516, Jules Verne University of Picardy, Amiens, France

[2] Medical Image Processing Department, Amiens Picardy University Hospital, Amiens, France

[3] Radiology Department, Amiens Picardy University Hospital, Amiens, France

[4] Neurosurgery Department, Amiens Picardy University Hospital, Amiens, France

Synopsis

Motivation

CSF dynamics is complex and regulates intracranial pressure. Pressure difference dynamics between the third and fourth ventricles (ΔP_t) drives CSF oscillations in the aqueduct. MRI can quantify aqueduct anatomy and CSF oscillations.

Goal

To quantify ΔP_t during free-breathing by combining MRI anatomical imaging with real-time phase-contrast MRI.

Approach

We developed a dedicated software to obtain: CSF flows dynamics Q(t), morphology of the aqueduct, its flow resistance (R) and ΔP_t which equal $Q_t \cdot R$. Cardiac and breathing contributions to ΔPt were investigated in volunteers.

Results

Contributions to ΔP_t were 12.3 Pa and 9.5 Pa from cardiac and breathing respectively.

Impact

Dedicated post-processing of real-time phase-contrast MRI allows quantification of CSF oscillations in the aqueduct and the pressure gradient between the third and fourth ventricles. Furthermore, continuous flow acquisition allows calculation of the cardiac and breathing influence on the pressure gradient.

Introduction

Cerebrospinal fluid (CSF) flow in the cerebral aqueduct is driven by the pressure difference (ΔP) between the third and fourth ventricles[1]. This ΔP can be calculated non-invasively by measuring the morphology of the aqueduct and the CSF flow through it[2-4]. However, precise morphological segmentation and post-processing of the images is currently a challenge for quantifying the ΔP. Furthermore, studies quantifying ΔP under breathing influence are lacking.

For this purpose, we have developed a highly automated platform (IDL language) that allows accurate quantitative analysis of cerebral aqueductal morphologies. This study aimed to use this platform, combined with continuous flow curves obtained from real-time phase-contrast MRI (RT-PC)[5,6], to quantify ΔP under cardiac and breathing influence.

Methods

Thirty-four healthy volunteers (age: 19-35) were examined using a clinical 3T scanner and a 32-channel head coil.

The cross-section of the aqueduct is nearly circular[7], and the hydrostatic effects are still dominant. In this study, we employed a two-dimensional projection of the aqueduct for morphological analysis and applied the Poiseuille formula to calculate ΔP. The equation $\Delta P = R \cdot Q$ comprises two crucial components: the resistance R (Fig.1-C) and the flow rate Q.

- **Calculation of Resistance**

The sagittal plane was imaged using the Balanced Fast Field Echo (BFFE) sequence with the parameters shown in Fig.1-A.

1. 2-3 images were selected for merging to obtain the aqueduct projection, and then linear interpolation was applied to increase the spatial resolution to $0.03 \times 0.03 mm^2$.
2. A line is manually drawn at the narrowest point of the aqueduct, and the software then automatically performs binary segmentation of the image based on the first-order derivative of the pixel's intensity profile.
3. Optionally, the platform supports mask inclusions (Fig.1-B).
4. The platform automatically delineates the boundary and centreline of the aqueduct, dividing it into multiple elements. Parameters such as length, diameter, angle, etc., are calculated for each element, along with its corresponding value of R (Fig.1-C).

- **Quantification of cardiac and respiratory flow rate**

Using in-house Flow[8-10] software for RT-PC post-processing:

1. The continuous flow signal was extracted through post-processing steps including image segmentation, background field correction and de-aliasing.
2. The flow signal was segmented into independent cardiac cycle flow curves (CCFC), interpolated to 32 points, and reconstructed into an average CCFC. The 95% limit of agreement (LOA) was calculated for this averaged CCFC (Fig.2-A).
3. Cardiac-induced flow variations corresponded to the extremes of the CCFC (QC_{Min} and QC_{Max}). In contrast, Breathing-induced flow variations (QB_{Min} and QB_{Max}) were defined by the difference between the extremes of the LOA and the extremes of the CCFC (Fig.2-B).

- **Quantification of cardiac and respiratory ΔP**

The ΔP was calculated by multiplying the obtained R with Q, representing the pressure difference between the fourth and third ventricles.

Results

Fig.3 shows that the CSF Reynolds number is below 2000, consistent with laminar flow characteristics; the mean Womersley number is 3. ΔPC_{Mean} was equal to 12.3±5.8 Pa, whereas ΔPB_{Mean} was equal to 9.5±7.2 Pa. ΔP_{BC} was equal to 78%.

Fig.4 illustrates the variation curve of the pressure gradient through the aqueduct, using ΔPC_{Mean} as an example. Fig.4-B shows that $|\Delta PC_{Min}| > \Delta PC_{Max}$, while ΔPB_{Max} is not significantly different from ΔPB_{Min}.

No correlation was observed between the aqueduct diameters obtained from RT-PC and BFFE (Fig.5-A). Instead, resistance correlates with RatioΔP_{BC}. Analysis of Fig.5-B reveals a negative correlation of resistance with QC_{Mean} and no correlation with QB_{Mean}, suggesting that resistance affects flow from cardiac sources but not from respiratory sources.

Discussion

Finite element segmentation of aqueduct morphology is crucial for accurately quantifying interventricular pressure. This platform streamlines the process and improves the accuracy of quantification. Future analysis of dynamic effects using Navier-Stokes equations is also possible due to its high scalability[11].

The breathing effect plays a significant role in quantifying the interventricular pressure difference, accounting for 78% of the cardiac-induced ΔP. Breathing-driven flow (QB) appears to be unaffected by changes in resistance, suggesting a decoupling from low-frequency respiratory influences, which is interesting to investigate. Breath-induced pressure changes may have significant clinical potential.

Conclusion

By combining anatomical MRI imaging with real-time phase-contrast MRI, it is possible to quantify the pressure difference between the third and fourth ventricles (ΔP) that drives CSF oscillations in the aqueduct. We have developed dedicated software for this purpose. Using continuous temporal acquisition of CSF flows in young healthy populations, we defined a reference physiological ΔP. We also quantified how cardiac and breathing functions influence this pressure. Such studies could contribute to a better understanding of the physiopathology of idiopathic hydrocephalus and hypertensive disorders.

Figures

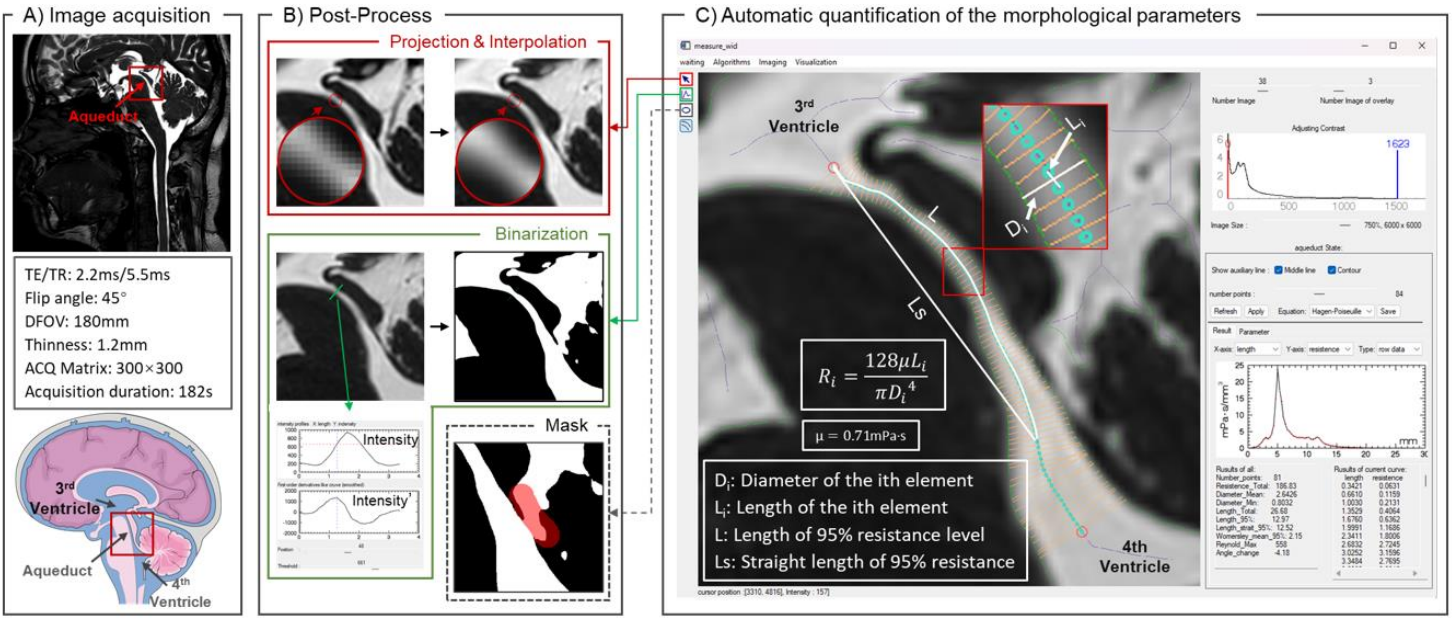

Figure 1: A) BFFE morphological images and associated parameters. B) Post-processing for cerebral aqueduct resistance quantification. Spatial resolution enhancement, automatic image binarization and mask inclusion. C) The software automatically performs a finite element analysis of the aqueduct to derive the resistance of each element. The 95% of the total resistance is then selected as the endpoint. Parameters such as resistance, mean diameter and length were extracted.

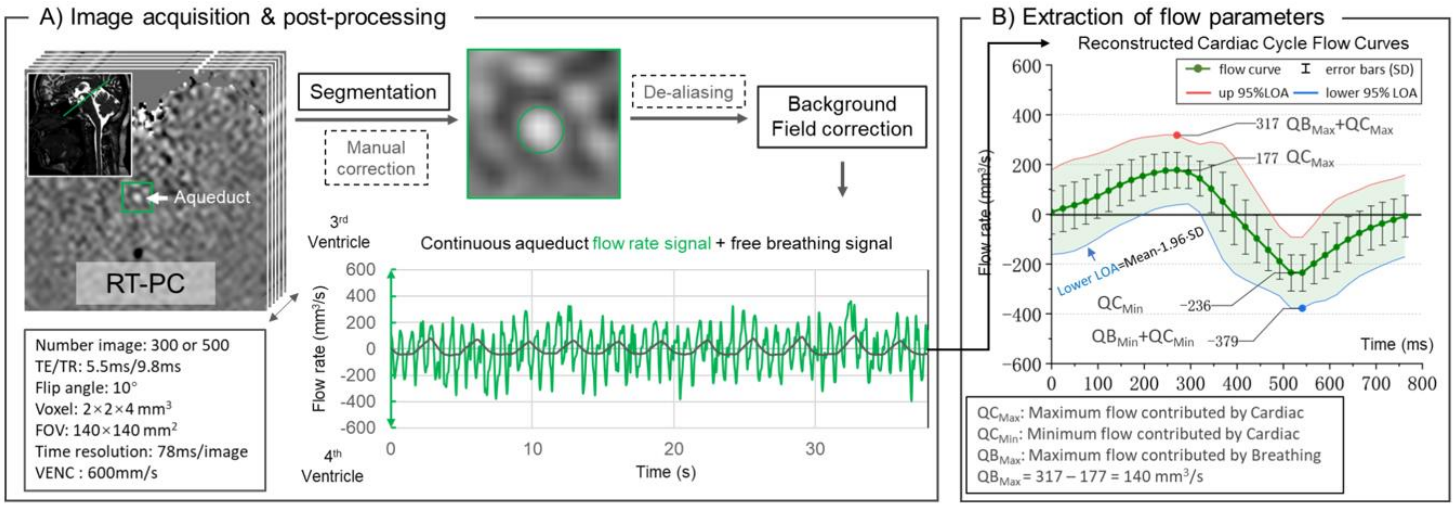

Figure 2: A) RT-PC MRI imaging levels and parameters. Continuous flow signal was obtained after post-processing, with the flow direction toward the third ventricle considered positive. B) The continuous flow signal was reconstructed as an averaged CCFC with a 95% LOA. The extremes of CCFC indicate cardiac-driven flow (QC_{Max} & QC_{Min}), and the differences between the extremes of LOA and the extremes of CCFC indicate breathing-driven flow (QB_{Max} & QB_{Min}). The Q_{Mean} = $(Q_{Max}+|Q_{Min}|)/2$.

A) Parameters from morphological images

Unit	Resistance (mPa·s/mm³)	Diameter mean (mm)	Diameter min (mm)	Diameter RT-PC (mm)	Length (mm)	Length strait (mm)	$Womersley_{mean}$ -	$Reynold_{max}$ -	Net flow (mm³/s)	Stroke Volume (mm³)
Mean ± SD	78 ± 51	2.7 ± 0.4	1.2 ± 0.2	2.9 ± 1.5	16.5 ± 3.2	15.7 ± 2.9	3.1 ± 0.5	254 ± 97	-1.8 ± 18.7	78.9 ± 29.5
Range	(24–253)	(1.7–3.6)	(0.8–1.8)	(2.0–3.6)	(10.4–23.6)	(10.1–22)	(2.2–5.0)	(98–504)	(-84–31.4)	(24–184)

B) Flow rate and ΔP (Contributions of Cardiac and Breathing)

Unit	Q_{Max} (mm³/s)	Q_{Min} (mm³/s)	ΔP_{Max} (Pa)	ΔP_{Min} (Pa)	ΔP_{Mean} (Pa)
Cardiac contributed	172 ± 74 (56–402)	-193 ± 86 -(67–459)	11.5 ± 5.9 (3.4–30)	-13.0 ± 6.1 -(2.9–26)	12.3 ± 5.8 (3.3–28)
Breathing contributed	127 ± 48 (47–235)	-121 ± 55 -(55–318)	9.7 ± 6.9 (2.3–36)	-9.3 ± 7.8 -(1.7–42)	9.5 ± 7.2 (2.4–38)
(Breathing/Cardiac)% + Wilcoxon's *p*	74% *	63% * *	84% *	72% **	78% **
Spearman's rho + *p* (Breathing vs. Cardiac)	0.35 *	0.47 **	0.61 **	0.76 **	0.75 **

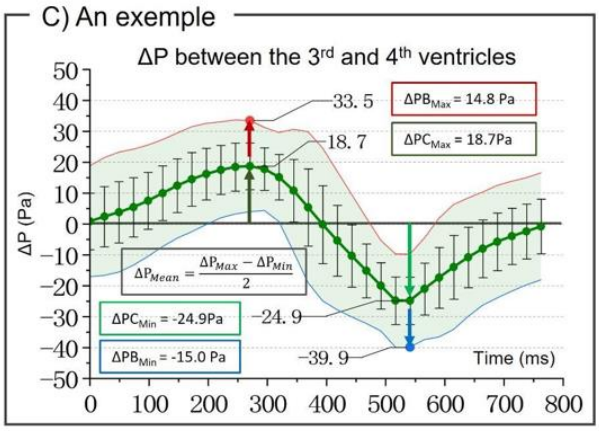

Figure 3: Results of morphological parameters in A) and flow and interventricular pressure (ΔP) in B). Definitions of some parameters are provided in C). Diameter RT-PC represents the diameter measured in the RT-PC image. Stroke volume is calculated as the sum of volume to skull and volume to extracranial. Analysis was performed using the Wilcoxon test and Spearman's test. * indicates $p<0.05$, ** $p<0.01$. Pulsatility refers to the ratio between amplitude and mean flow.

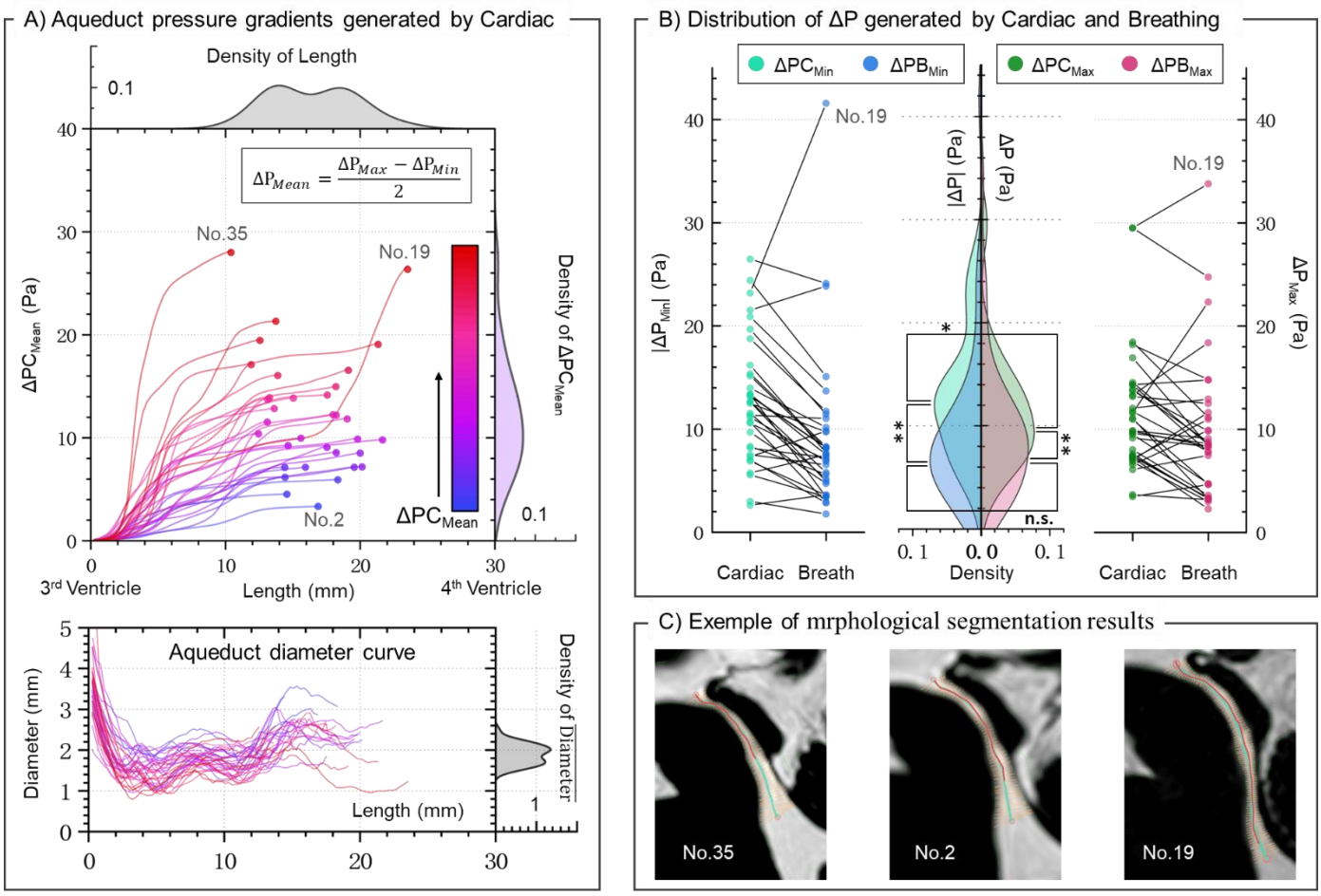

Figure 4: A) Aqueduct pressure gradient (ΔPC_{Mean}) curve (top) and aqueduct diameter profile as a function of length (bottom). B) Distribution of cardiac- and breathing-induced ΔP. ΔPC_{Max} represents the cardiac-induced pressure difference from the fourth to the third ventricle. The distribution of the four parameters in the densitogram is shown in the middle. C) Morphological segmentation results of three volunteers. (* The part B) has been corrected in this version to address the error present in the original image)

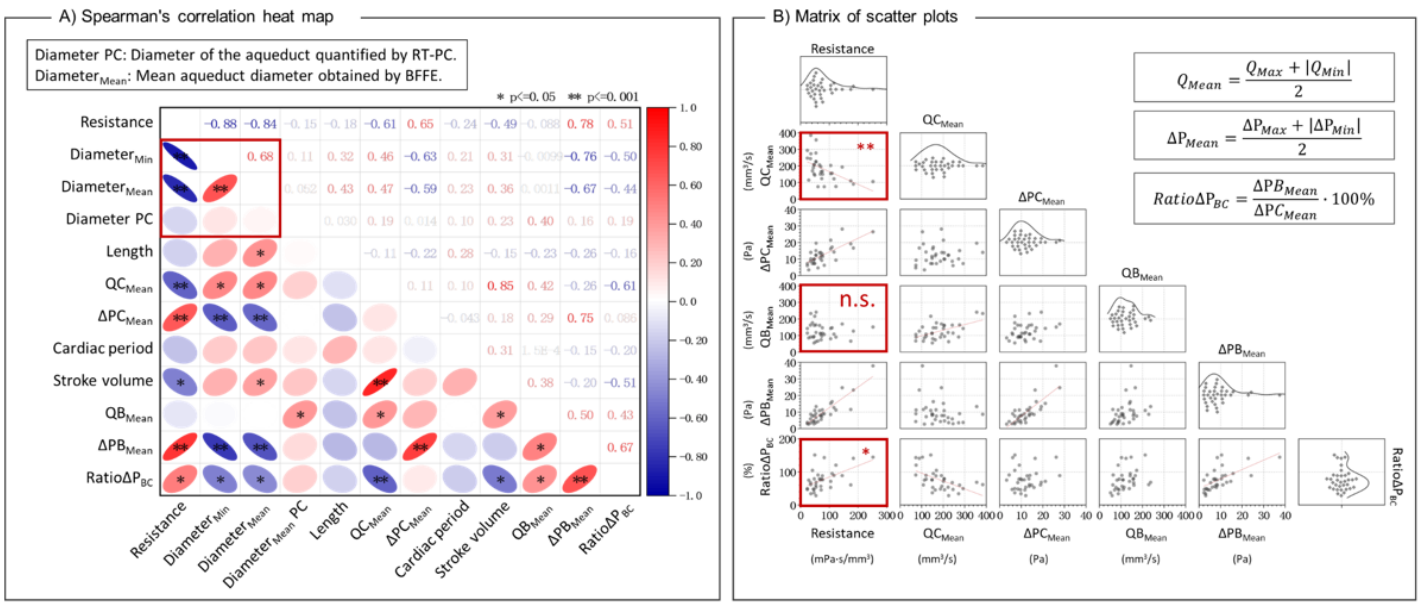

Figure 5: A) Heat map of Spearman's correlation of several parameters, the diameter collected by RT-PC is not correlated with the mean diameter collected by BFFE. The resistance is correlated with the mean diameter and the length collected by BFFE. B) Matrix of scatter plots of the resistance R, the flow rate Q, and the pressure difference ΔP. Resistance is negatively correlated with QC (cardiac-derived flow) and not correlated with QB.

References

1. Sincomb S, Coenen W, Sánchez AL, Lasheras JC. A model for the oscillatory flow in the cerebral aqueduct. Journal of Fluid Mechanics. 2020 Sep;899:R1. https://doi.org/10.1017/jfm.2020.463.

2. Sincomb S, Moral-Pulido F, Campos O, Martinez-Bazan C, Haughton V, Sánchez AL. An In-Vitro Experimental Investigation of Oscillatory Flow in the Cerebral Aqueduct. Research Square. 2023 Apr 3. https://doi.org/10.2139/ssrn.4564789.

3. Bardan G, Plouraboué F, Zagzoule M, Balédent O. Simple patient-based transmantle pressure and shear estimate from cine phase-contrast MRI in cerebral aqueduct. IEEE transactions on biomedical engineering. 2012 Aug 8;59(10):2874-83.

4. Markenroth Bloch K, Töger J, Ståhlberg F. Investigation of cerebrospinal fluid flow in the cerebral aqueduct using high-resolution phase contrast measurements at 7T MRI. Acta Radiologica. 2018 Aug;59(8):988-96.

5. Liu P, Fall S, Ahiatsi M, Balédent O. Real-time phase contrast MRI versus conventional phase contrast MRI at different spatial resolutions and velocity encodings. Clinical Imaging. 2023 Feb 1;94:93-102. https://doi.org/10.1016/j.clinimag.2022.11.015.

6. Chen L, Beckett A, Verma A, Feinberg DA. Dynamics of respiratory and cardiac CSF motion revealed with real-time simultaneous multi-slice EPI velocity phase contrast imaging. Neuroimage. 2015 Nov 15;122:281-7. https://doi.org/10.1016/j.neuroimage.2015.07.073.

7. Fin L, Grebe R. Three dimensional modeling of the cerebrospinal fluid dynamics and brain interactions in the aqueduct of sylvius. Computer methods in biomechanics and biomedical engineering. 2003 Jun 1;6(3):163-70. https://doi.org/10.1080/1025584031000097933

8. Liu P, Lokossou A, Fall S, Makki M and Bamendent O, 2019. Post Processing Software for Echo Planar Imaging Phase Contrast Sequence. ISMRM 27th, (4823). https://archive.ismrm.org/2019/4823.html

9. Balédent O, Idy-peretti I. Cerebrospinal fluid dynamics and relation with blood flow: a magnetic resonance study with semiautomated cerebrospinal fluid segmentation. Investigative radiology. 2001 Jul 1;36(7):368-77.

10. Liu P, Fall S, Balédent O. Flow 2.0-a flexible, scalable, cross-platform post-processing software for realtime phase contrast sequences. In ISMRM 2022-International Society for Magnetic Resonance in Medicine 2022 May 7. https://archive.ismrm.org/2022/2772.html

11. Jacobson EE, Fletcher DF, Morgan MK, Johnston IH. Fluid dynamics of the cerebral aqueduct. Pediatric neurosurgery. 1996 Mar 7;24(5):229-36. https://doi.org/10.1159/000121044

Acknowledgements

This research was supported by EquipEX FIGURES (Facing Faces Institute Guilding Research), Hanuman ANR-18-CE45-0014 and Region Haut de France.

Thanks to the staff members at the Facing Faces Institute (Amiens, France) for technical assistance.

Thanks to David Chechin from Phillips industry for his scientific support.